Kinetic and Structural Properties of Disulfide Engineered Phospholipase A₂: Insight into the Role of Disulfide Bonding Patterns[†,‡]

Bao-Zhu Yu,[§] Ying H. Pan,[§] Marcel J. W. Janssen,[‖,⊥] Brian J. Bahnson,*,[§] and Mahendra K. Jain*,[§]

Department of Chemistry & Biochemistry, University of Delaware, Newark, Delaware 19716, and Department of Enzymology and Protein Engineering, Utrecht University, Utrecht, The Netherlands

Received August 17, 2004; Revised Manuscript Received December 7, 2004

ABSTRACT: The family of secreted 14 kDa phospholipase A₂ (PLA2) enzymes have a common motif for the catalytic site but differ in their disulfide architecture. The functional significance of such structural changes has been analyzed by comparing the kinetic and spectroscopic properties of a series of disulfide mutants engineered into the sequence of pig pancreatic IB PLA2 to resemble the mammalian paralogues of the PLA2 family [Janssen et al. (1999) *Eur. J. Biochem. 261*, 197−207, 1999]. We report a detailed comparison of the functional parameters of pig iso-PLA2, as well as several of the human homologues, with these disulfide engineered mutants of pig IB PLA2. The crystal structure of the ligand free and the active site inhibitor-MJ33 bound forms of PLA2 engineered to have the disulfide bonding pattern of group-X (eng-X) are also reported and compared with the structure of group-IB and human group-X PLA2. The engineered mutants show noticeable functional differences that are rationalized in terms of spectroscopic properties and the differences detected in the crystal structure of eng-X. A major difference between the eng-mutants is in the calcium binding to the enzyme in the aqueous phase, which also influences the binding of the active site directed ligands. We suggest that the disulfide architecture of the PLA2 paralogues has a marginal influence on interface binding. In this comparison, the modest differences observed in the interfacial kinetics are attributed to the changes in the side chain residues. This in turn influences the coupling of the catalytic cycle to the calcium binding and the interfacial binding event.

Molecular cloning studies (*3*, *4*) have shown that humans contain at least 9 genes and mice contain 10 genes that encode proteins in the 14 kDa secreted phospholipase A₂ (PLA2)[1] family. The pattern of tissue distribution of the PLA2 paralogues within an organism suggests specific
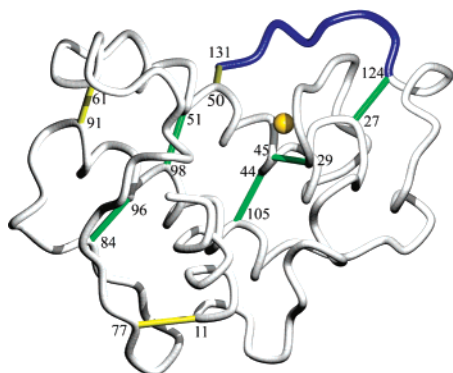
* Address correspondence to M.K.J. (phone, 302-831-2968; e-mail, mkjain@udel.edu) or B.J.B. (phone, 302-831-0786; e-mail, bahnson@udel.edu).

[§] University of Delaware.

[‖] Utrecht University.

[⊥] Current address: Department of Clinical Chemistry, Academic Medical Center, 1100 DD Amsterdam, The Netherlands.

[1] Abbreviations: CMC, critical micelle concentration; deoxy-LPC, 1-hexadecyl-2-deoxy-glycerophosphocholine; D-LPC, 3-hexadecyl-1-glycerophosphocholine; DMPM, dimyristoylglycero-*sn*-3-phosphomethanol; EA, *trans*-elaidoylamide; eng-mutants, the disulfide engineered porcine group-IB PLA2 with the disulfide architectures shown in Figure 1; HDNS, *N*-dansyl-hexadecyl-phosphoethanolamine; hPLA2, paralogues of human PLA2 such as hX; i-face, interface binding surface; iso-PLA2, pig IB PLA2 with natural (A12T,H15D,M20L,E71N) substitutions; MJ33, 1-hexadecyl-3-(trifluoroethyl)-*sn*-glycero-2-phosphomethanol; PC₆-ether, 1,2-dihexyl-glycero-*sn*-3-phosphocholine; PCU, (*R*)-2-*O*-decanoylamino-octanol-1-*O*-phosphocholine; PGU, (*R*)-2-*O*-decanoylamino-octanol-1-*O*-phosphoglycol; OA, *cis*-oleoylamide; PLA2, 14 kDa secreted phospholipase A₂; PN16, *n*-hexadecyl-1-phosphocholine; RET, resonance energy transfer; TMA-DPH, *p*-trimethylammonium diphenylhexatriene; X1, masticadienoic acid; X_I^{50*}, inhibitor mole fraction in the substrate interface for half activity. Parameters have their standard enzymological significance except that those marked with an asterisk relate to the process in the interface (*1*, *2*).

biological roles that remain to be characterized. Although all secreted PLA2 enzymes require calcium for the turnover, quantitative differences in the calcium binding and interface preference are significant (*5*). In addition to the sequence variation, the family of PLA2 enzymes also have significant structural differences in the location and patterns of their 5 to 8 disulfide bridges. In order to dissect the functional consequences of such differences Janssen et al. (*6*) engineered a set of mutants from the sequence of the M8,20L mutant of the wild-type IB pig pancreatic PLA2. In these eng-mutants the disulfide bridges (Figure 1) are in the positions corresponding to their human homologue.

In this paper we report a kinetic characterization of five of the engineered mutants (eng-IIA, eng-IIB, eng-IIC[#], eng-V, and eng-X). These results are compared with those of the wild-type pig IB PLA2, its natural variant iso-PLA2 (A12T, H15D, M20L, E71N), and five of the human enzymes (hIB, hIIA, hV, hX, hXII). The crystal structures of the ligand free and an inhibited form of eng-X are also presented and compared with the previously reported structures of wild-type pig IB (*7*) and hX PLA2 (*8*). These results show that the disulfide architecture has a significant effect on the calcium binding and the associated active site events without displaying a significant effect on the functions of the interface binding region (i-face) of PLA2.

EXPERIMENTAL PROCEDURES

Human PLA2s were kindly provided by Professor Michael Gelb (University of Washington, Seattle). The eng-mutants

| | | disulfide | |
group	11-77	61-91	50-131
IB	yes	yes	no
V	no	yes	no
X	yes	yes	yes
IIA	no	yes	yes
IIB	no	no	yes
IIC[#]	no	yes	yes

FIGURE 1: Altered disulfide bridges (in yellow) for the eng-mutants of (M8,20L)-IB pig pancreatic PLA2 are shown relative to the structure of eng-X with sequence numbering relative to the IB enzyme. The disulfide bridges 27−124, 29−45, 44−105, 51−98, 84−96 (in green) are common to each paralogue. The C-terminal extension (residues 124−131, KGESDKC) is marked in blue, and a three residue insertion present in IIC[#] (residue N88 replaced with the 3 residues GSG) is not shown (6). The variant S−S bridges (yellow) in the eng-PLA2s were introduced by introducing Ser for Cys at 77 or 91, C50N, and/or the C-term extension (tabulated above).

were expressed, purified, and characterized as described previously (6). Wild-type pig IB PLA2 and iso-PLA2 (A12T,H15D,M20L,E71N) were purified from acetone powder of pig pancreas (9). The experimental and analytic basis for the assays has been described (1, 2, 10−12). The fluorescence measurements on SLM-Aminco AB2 were done with 1 or 2 μM PLA2 in a stirred 1.6 mL buffer in a 1 cm cuvette (13). The slit widths were 4 nm with excitation at 280 nm and emission at 333 nm. All kinetic and spectroscopic measurements were performed at 24 °C and pH 8.0 under conditions further specified in the figure captions and the text. Statistical uncertainty in the reported measurements is 10%, and it is 30% in the calculated parameters.

Crystallization and X-ray Data Collection. Protein crystal growth experiments were designed to obtain crystals of the Ca-coordinated eng-X enzyme with and without the bound competitive inhibitor 1-hexadecyl-3-(trifluoroethyl)-*sn*-glycero-2-phosphomethanol (MJ33). Protein crystal screening of eng-X was carried out using the hanging drop method (14) at 25 °C and commercially available crystallization screens (Hampton Research). For the MJ33-complexed crystals the hanging drops were made by mixing 2.0 μL of a stock solution containing 15 mg/mL eng-X, 10 mM CaCl$_2$, and 3 mM MJ33 with 2.0 μL of a reservoir solution of 0.2 M ammonium sulfate, 30% w/v polyethylene glycol 8000, and 0.1 M Na$^+$-cacodylate, pH 6.5. The MJ33-free crystals of eng-X were obtained by mixing 2.0 μL of the same protein stock solution containing 3 mM MJ33, as above, but with 2.0 μL of a reservoir solution of 10% w/v 2-propanol, 20% w/v polyethylene glycol 4000, and 0.1 M Na$^+$-Hepes, pH 7.5 (i.e. MJ33 does not bind in the presence of 2-propanol).

X-ray diffraction data sets for the two eng-X crystal forms were collected on a Rigaku-RUH3R rotating anode generator with a RAXIS IV image plate area detector. For the eng-X crystal form with bound MJ33, two crystals were needed to collect a complete data set, due to X-ray induced damage under the cryo conditions (−180 °C). Otherwise, both the crystal forms were pretreated in a similar fashion. Each required the introduction of a cryosolution made of the crystallization condition reported above with the addition of glycerol as the cryoprotectant at a concentration of 10%, then flash frozen in the −180 °C nitrogen cryostream. The programs DENZO and SCALEPAK (15) were used for data processing and scaling.

Molecular Replacement. Molecular replacement was performed using the program AMORE (16) to solve the crystal structure of eng-X. The structure was first solved for the eng-X crystal form with space group symmetry $P2_1$ without bound MJ33. The porcine group-IB PLA2 model (PDB 1FXF) was used as the initial search model. Residues 60−70 were originally deleted from the search model due to packing interferences when the complete model was used. Two independent solutions were found in the rotational search with a peak intensity well above the noise level. The translation search gave a unique solution of 2 subunits within the asymmetric unit and with a final correlation factor of 38.5% and R-factor of 0.455. The partially refined eng-X model was then used to solve the structure of the MJ33-bound crystal form ($P2_1$). This crystal form had an altered arrangement of 2 subunits of eng-X in the asymmetric unit, and the translation search gave a final correlation factor of 42.4% and an R-factor of 0.451.

Crystallographic Refinement. Standard refinement procedures using the program CNS (17) were successful in obtaining a reliable model of the eng-X PLA2 structure with and without bound MJ33. Iterative model improvement and refinement was done using the programs CHAIN (18) and O (19). In refining the structure of the MJ33-free form in space group $P2_1$, the initial model obtained from molecular replacement was subjected to a round of rigid-body, positional, individual temperature factor (B-factor) and simulated annealing (5000 °K) refinement to a resolution of 2.5 Å, resulting in an R_{free} value of 0.474 and an $R_{working}$ value of 0.388 (20). At this point, the missing sequence from the search model of porcine IB PLA2 was introduced into the model and the site-directed changes M8L, M20L, and N50C were incorporated. The C-terminal extension of KGESDKC is what distinguishes eng-X from the group-IB PLA2. This extension, which became residues 125−131, was added to model the disulfide bonding pattern of the group-X enzyme (6). These residues were next added to the model. After one round of positional and simulated annealing refinement the R_{free} and $R_{working}$ were 0.415 and 0.335, respectively. With 216 solvent molecules built into the model and extending the resolution to 2.25 Å, the final R_{free} was 0.265 and $R_{working}$ were 0.191 with good geometry. Refinement of the crystal form with bound MJ33 was more straightforward, starting from the nearly final model from the ligand-free crystal form of eng-X PLA2. The model was refined to a resolution of 2.00 Å, and included 206 waters added to the model, yielding an R_{free} and $R_{working}$ of 0.245 and 0.196, respectively, with good geometry.

Table 1: The Interfacial Kinetic Parameters for the PLA2 Disulfide Engineered Pig IB Mutants Compared to the Natural Human Homologues

Pig IB Mutant

	DMPM			DC$_7$PC^d 4 M NaCl			DC$_7$PC^d 1 mM NaCl	DC$_6$PC monodisperse
	v_0 (s^{-1})^a	O/S^b	X_I^{50*} ^{c}	V_M^{app} (s^{-1})	K_M^{app}	X_I^{50*} ^{c}	V_M^{app} (s^{-1})	v^{mono} (s^{-1})^e
WT	270	10	0.006	660	0.2	0.012	16	<0.1
iso-PLA2	65	8	0.039	194	0.2	0.015	64	
M8,20L	185	11	0.01	270	0.2	0.013	5	0.8
eng-IIA	130	10	0.009	105	0.5	0.015	0.1	0.2
eng-IIB	50	4.5	0.009	15	0.3	0.064	0.1	<0.1
eng-IIC#	45	4.5	0.01	17	0.48	0.054	0.1	<0.1
eng-V	150	12	0.008	117	0.18	0.02	0.1	0.06
eng-X	125	11	0.006	160	0.24	0.016	2.4	0.05

Human PLA2s

	DMPM			DC$_7$PC^d 4 M NaCl			DC$_7$PC^d 1 mM NaCl	DC$_7$PC monodisperse
	v_0 (s^{-1})^a	O/S^b	X_I^{50*} ^{c}	V_M^{app} (s^{-1})	K_M^{app}	X_I^{50*} ^{c}	V_M^{app} (s^{-1})	v^{mono} (s^{-1})^e
hIB	135	10	0.008	55	0.74	0.1	31	3
hIIA	33	3.8	0.01	200	0.32	0.25	18	1.8
hV	3.4	1.2	0.05	31			12	7
hX	10	3.3	0.05	34	0.12	>0.5	45	24
hXII	3.5		0.05	10			12	0.9

^{a} The initial rate v_0 at a DMPM mole ratio of $X_S^* = 1$ was measured under a standard assay protocol with Ca^{2+} at 0.5 mM (21−24). Statistical uncertainty in the reported measurements is 10%, and it is 30% in the calculated parameters. ^{b} The ratio of DMPM hydrolysis versus the *sn*-1,2-dithio-analogue of DMPM. ^{c} The X_I^{50*} is the mole fraction of the competitive inhibitor 1-hexadecyl-3-(trifluoroethyl)-*sn*-glycero-2-phosphomethanol (MJ33), which gave 50% inhibition. ^{d} The DC$_7$PC assays were performed in the presence of 5 mM Ca^{2+}. ^{e} The v^{mono} results are in 0.4 mM DC$_n$PC with 5 mM Ca^{2+} in fluorometric assay with pH indicatory assay (30).

RESULTS

A necessary precondition for ensemble averaging for enzyme kinetics is that the defined turnover path should remain invariant during the observed reaction progress. Coupled with the requirement for the microscopic steady state, such restrictions pose challenges for the analysis of the observed steady state reaction progress by interfacial enzymes (1, 2). To circumvent such difficulties we have developed assays where the observed reaction progress occurs processively only through the steps of the interfacial Michaelis−Menten turnover path. Established protocols are used in this paper to characterize the effects of the structural changes in the eng-PLA2 mutants and the human PLA2 enzymes that they are compared to (1, 2).

Apparent Rate of Hydrolysis at $X_S^* = 1$. The interfacial kinetic parameters for the eng-mutants and the human PLA2 enzymes are summarized in Table 1. From a zero-order reaction progress in the highly processive scooting mode bound to DMPM vesicles (11), the initial rate v_0 at $X_S^* = 1$ is obtained in the presence of polymyxin B that mediates a rapid and direct vesicle−vesicle exchange of DMPM on the enzyme containing vesicles (21−24). Likewise, the V_M^{app} at $X_S^* = 1$ is the maximum rate with the saturating concentration of DC$_7$PC micelles in 4 M NaCl (12). In this assay at 4 M NaCl, preferential partitioning of chloride in the

zwitterionic interface promotes binding and interfacial activation of the bound enzyme. During this processive interfacial turnover the substrate replenishment is rapid, such that the chemical step for the turnover by the interfacially bound and activated PLA2 remains rate-limiting. In contrast, in 1 mM NaCl the enzyme does not bind as tightly and is not interfacially activated by anionic charge. Here the V_M^{app} at saturating DC$_7$PC is related to the fraction of the bound enzyme that is interfacially activated (25, 26).

Results in Table 1 show that the rates of hydrolysis of both the substrates at $X_S^* = 1$ by the eng-mutants are significantly different: The range is 45 to 270 s^{-1} for the hydrolysis of DMPM vesicles in 0.5 mM calcium, and 15 to 660 s^{-1} for the hydrolysis of DC$_7$PC micelles in 4M NaCl and 10 mM calcium. The rate of hydrolysis of DC$_7$PC micelles in 1 mM NaCl is significantly lower. Together these results show that the eng-mutants are activated by the interfacial anionic charge which is consistent with the proposed role of lysine or arginine residues in positions 53, 56, 57, 120, and 121 in the k_{cat}^* activation by the interfacial anionic charge (26).

The initial rates of hydrolysis of the anionic DMPM vesicles at $X_S^* = 1$ by the human PLA2s are also different. These rates are typically 2- to 6-fold higher than the observed rates in the fatty acid displacement assay with 1-palmitoyl-2-oleoyl-phosphatidylglycerol (5, 27, 28). It is likely that the rate difference could be due to substrate specificity. However, for at least pig IB PLA2, there does not appear to be such specificity. On the basis of the consideration of the variables in the microenvironment of the bound enzyme in displacement assay we attribute the observed difference to a combination of the effectively lower X_S^*, the inhibition from the added fatty acid probe, and the accumulated product. The X_I^{50*} mole fraction values for 50% inhibition of the human enzymes are higher in the displacement assay than those reported here (see below). This is predicted if the apparent K_M^* is lower due to the accumulation of the product. This is because the dependence of the X_I^{50*} on the substrate and inhibitor mole fraction is related to the intrinsic affinity or K_I^* for the active site directed competitive inhibitor, as well as K_M^* and K_P^* (1, 2, 29).

In addition, the rates of hydrolysis of DC$_7$PC micelles in 1 mM NaCl by the human PLA2s are significantly different. Higher rates for the hX and hV suggest that these enzymes do not require anionic charge for the interfacial activation. This is consistent with the result that no activation is seen in 4 M NaCl. Conversely, rate enhancement in 4 M NaCl is observed with hIB and hIIA, which is consistent with the presence of the cationic residues in positions 53, 56, and 120 of the hIB and hII enzymes (25, 26).

The rate of hydrolysis of monodisperse 0.44 mM DC$_6$PC or DC$_7$PC under the unstirred conditions is given as v^{mono}. As shown elsewhere (30), v^{mono} values do not necessarily provide evidence for the turnover path via the classical ES in the aqueous phase (30). Significant turnover with unstirred monodisperse substrate can also be due to the formation of premicellar aggregates of the interfacial enzymes, whereas the rate in the stirred reaction mixture will also have contribution from the reaction on the extraneous surfaces such as the vessel walls and the air bubbles. For such reasons, significant rates of hydrolysis of monodisperse DC$_6$PC or DC$_7$PC in the aqueous phase (30) seen only with some of
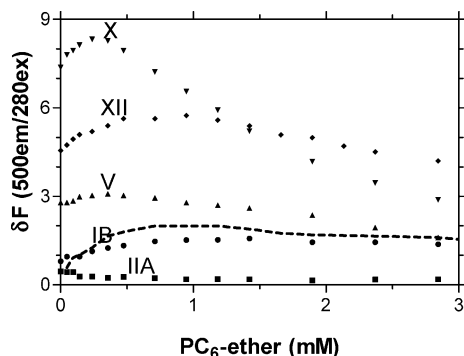
FIGURE 2: The change in the RET signal from 1 μM HDNS and 1 μM human PLA2 enzymes with added dihexyl-phosphatidyl-choline (PC$_6$-ether). The number of tryptophan residues is one in IB, none in IIA, four in hV, two in hX, and three in XII. Results for the eng-X are shown as the dashed line.
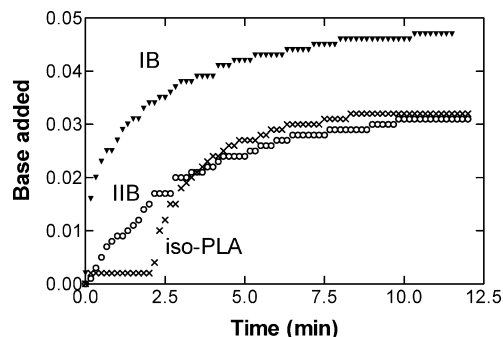

FIGURE 3: Reaction progress for the hydrolysis of DMPM (600 nmol) sonicated vesicles by 15 pmol of PLA2s: (triangles) IB-WT, (crosses) eng-IIB, and (circles) iso-PLA2. On the ordinate, a change of 0.01 corresponds to 1.15 nmol of base added. Note that the curve for the IB-WT enzyme is vertically shifted, and the curve for iso-PLA2 is horizontally shifted. The extent of hydrolysis per enzyme is virtually identical with all the PLA2s and corresponds to the size of vesicles (*33*).

the human PLA2s (v^{mono} in Table 1) are attributed to the formation of premicellar complexes (*8*).

Results in Figure 2 provide evidence for the formation the premicellar complex. The resonance energy transfer from a dansyl acceptor is significant when the resonance energy transfer acceptor *N*-dansyl-hexadecyl-phosphoethanolamine (HDNS) is bound to PLA2. The resonance energy transfer (RET) signal increases further at low concentrations of added monodisperse dihexadecyl phosphatidylcholine (PC$_6$-ether, CMC = 3 mM) and then decreases as HDNS is competed out from the complex by excess PC$_6$-ether monomers. In comparison the change in the RET signal is insignificant with hIB and also with all the eng-mutants. Results with hIIA provide a useful control because this PLA2 does not have the Trp-donor. Although the RET results cannot be quantitatively interpreted (*13, 31*), results in Figure 2 provide clear evidence for the binding of HDNS to certain human PLA2 as well as for the formation of the premicellar complexes of some of the human PLA2s with PC$_6$-ether.

The catalytic mechanism for the eng-mutants likely remains unchanged because the O/S ratio, for the rates of hydrolysis of DMPM versus the *sn*-1,2-dithio analogue of DMPM, is in the 8 to 12 range (Table 1). In contrast, the O/S ratio is significantly lower for eng-IIB and eng-IIC#, and also for most of the human PLA2s. These results suggest that the chemical step is rate-limiting if the O/S ratio is significantly different from unity (*32*). On the basis of the evidence developed later we suspect that the differences in the O/S ratio are possibly due to the differences in the partitioning of the Michaelis complex E*S into E*P and E* + S*.

The first-order reaction progress is characteristic for the processive interfacial turnover in the scooting mode (*10*). Results for the hydrolysis of DMPM vesicles by three different mutants are shown in Figure 3, and comparable results were obtained with all the mutants and the human PLA2s (not shown). In such scooting mode reaction progress curves the extent of hydrolysis corresponds to the fraction of the vesicle population with bound enzyme as predicted by the Poisson distribution of the enzyme monomer over the total vesicle population (*23*). Under the conditions of Figure 3, with a >6-fold excess of vesicles per enzyme, the amplitude of hydrolysis corresponds to the vesicle size (*11, 33*), and it is virtually the same for the mutants. These results show that the bound eng-mutant does not leave the DMPC

vesicle interface during the processive turnover. In the time scale of the experiment, the enzyme remains confined to its original vesicle even when all the available substrate on the vesicle has been hydrolyzed. Thus on the basis of results in Figure 3 we conclude that a more than 5-fold difference in the v_0 values for eng-IB and eng-IIB (Table 1) is not due to a difference in the amount of inert or inactive enzyme present as impurity in the protein preparation.

Kinetic X_I^{50*} for the Active Site Directed Ligands. Hydrolysis by eng-mutants and the human PLA2s normally requires calcium. It can be replaced by cobalt(II), but not by Zn(II). As previously reported, both of these results are due to substitution of calcium by these divalent cations (*34*). As summarized in Table 2 Zn(II) is a potent inhibitor of the eng-mutants with the 50% inhibitory concentration in the 1−2 μM range for the hydrolysis of DMPM vesicles in the presence of 500 μM calcium.

Results in Table 1 show that the inhibitory potency of the *sn*-2-tetrahedral mimic MJ33 is virtually the same with eng-mutants but not with the human PLA2s. The X_I^{50*} values, the mole fraction of MJ33 for the 50% inhibition, is between 0.006 and 0.01 for hydrolysis of DMPM vesicles, and 0.03 to 0.06 mole fraction for the hydrolysis of DC$_7$PC micelles. On the basis of the relation in eq 1 (*1, 2*), either K_M^* and

$$\frac{v_0}{v_I} = 1 + \left(\frac{1 + \dfrac{1}{K_I^*}}{1 + \dfrac{1}{K_M^*}}\right)\left(\frac{X_I^*}{1 - X_I^*}\right) \qquad (1)$$

K_I^* for the mutants are not different or they somehow compensate for each other. At $v_0/v_I = 2$, $X_I^{50*} = [1 + 1/K_M^*]/[1 + 1/K_I^*]$. Since the K_M^{app} values for the hydrolysis of DC$_7$PC micelles, related to K_M^* for the mutants, change modestly, we believe that at least some of the effect of mutation is on K_M^*. This would imply that parallel changes in K_M^* and K_I^* compensate so that the X_I^{50*} values for the eng-mutants do not change significantly.

The above interpretation is also consistent with other results in Table 2: X_I^{50*} values for several potent inhibitors are virtually the same for the eng-mutants, and the values are significantly different for the human PLA2s. For example, the X_I^{50*} values for PGU or PCU (the glycero-*sn*-2-amide

Table 2: X_I^{50*} Values for eng-Mutants for the Initial Rate of Hydrolysis of DMPM Vesicles[a]

	PGU	PCU	OA	EA	X1	deoxy-LPC	D-LPC	PN16	Zn^{2+} (μM)
					Pig IB Mutant				
WT	0.0025	0.013	0.003	0.006	0.009	>1.6	1.2	1	0.9
iso-PLA2	0.005	0.040	0.009	0.023	0.010	>1	1	0.80	1.2
M8,20L	0.002	0.013	0.006	0.01	0.020	0.16	0.30	0.30	
eng-IIA	0.001	0.036	0.006	0.006	0.054	0.80	1	1	
eng-IIB	0.0025	0.017	0.006	0.008	0.015	0.09	0.05	0.11	
eng-IIC[#]	0.0023	0.035	0.006	0.010	0.040	0.09	0.05	0.14	
eng-V	0.0024	0.019	0.0044	0.007	0.021	0.50	0.09	1	
eng-X	0.0025	0.015	0.005	0.011	0.021	0.30	0.09	1	
					Human PLA2s				
hIB	0.009	0.010	0.014	0.025	0.017				1.7
hIIA	0.010	0.040	0.013	0.014	0.017				2.3
hV	0.033	0.0036	0.025	0.0078	0.060				2.1
hX	0.0058	0.0017	0.011	0.0055	0.055				2.5
hXII	0.059	0.035	0.060		0.009				0.9

[a] The X_I^{50*} is the mole fraction of the competitive inhibitor that gave 50% inhibition. Statistical uncertainty is 30% in the calculated value of the X_I^{50*}. The full chemical names of these inhibitors are given here: PGU, (*R*)-2-*O*-decanoylamino-octanol-1-*O*-phosphoglycol; PCU, (*R*)-2-*O*-decanoylamino-octanol-1-*O*-phosphocholine; OA, *cis*-oleoylamide; EA, *trans*-elaidoylamide; X1, masticadienoic acid; deoxy-LPC, 1-hexadecyl-2-deoxy-glycerophosphocholine; D-LPC, 3-hexadecyl-1-glycerophosphocholine; PN16, *n*-hexadecyl-1-phosphocholine. PCU and PGU were kindly provided by Professor deHaas (Utrecht).

analogue of the substrate) do not change with the disulfide architecture of the eng-mutants, and in all cases PGU is about 6-fold more potent than PCU. Also the range of X_I^{50*} values for oleoylamide (OA) is relatively narrow. However, the trans-analogue elaidoylamide (EA) appears to be discriminated better by the eng-mutants. Similar differences in the X_I^{50*} values for the inhibition of eng-mutants by X1 (masticadienoic acid or schinol) (*35*) are also significant. About half of this modest discrimination by the eng-mutants is attributable to the M8,20L substitution and the other half to the changes in the disulfide architecture.

Results in Table 2 show that there is a significant difference in the discrimination for the three phosphocholine analogues as the weak inhibitors of the engineered disulfide mutation: 1-hexadecyl-2-deoxy-glycerophosphocholine (deoxy-LPC), 3-hexadecyl-1-glycerophosphocholine (D-LPC), and hexadecyl-1-phosphocholine (PN16). The affinity of eng-IIB and eng-IIC[#] mutants for deoxy-LPC or D-LPC is 3 to 10 times greater than that of the other eng-mutants. These are weak inhibitors presumably because they do not have the *sn*-2-substituent that can interact with calcium or with the catalytic His-48. These results suggest that one of the effects of the disulfide architecture could be in the apparent discrimination of the (glycero)-phosphocholine headgroup. Since the X_I^{50*} values for the eng-mutants vary significantly, none of these weakly inhibitory phosphocholines can be used as a surface diluent for the determination of the K_I^* for the more potent inhibitors (*29, 36, 37*). These results dash our hope of finding a single surface diluent for all the eng-mutants. The limitation also precludes determination of K_M^* by available methods (*1, 2*), which could have provided a mechanistic basis for the differences in the v_0 and V_M^{app} values of the eng-mutants (Table 1).

Rate of Alkylation of the Catalytic Residue His-48. The rate of alkylation of His-48 in PLA2 changes upon the binding of calcium. The rate of alkylation is also influenced by the binding of the active site directed ligands which obligatorily requires calcium (*36*). Results in Table 2 suggest that the apparent affinity of the weaker inhibitors could be due to a lower affinity of calcium for the free E form of eng mutants. This is consistent with the results in Table 3, i.e.

Table 3: Active Site Histidine Alkylation Time for E and E* Forms of PLA2 and the Derived Dissociation Constants of Ca-Free PLA2 from Deoxy-LPC[a]

PLA2 form	t_E (min)	K_{Ca}^b (mM)	$K_{ND}^*(-Ca)^c$ (mM)
IB WT	9	0.32	>2
M8,20L	15	0.14	1.2
eng-IIA	45	1.5	>2
eng-IIC[#]	50	0.41	>1
eng-V	40	0.25	>2
eng-X	16.6	1.1	1

[a] The inactivation time by alkylation of His-48 by *p*-nitro-phenacyl-bromide (*36*). Statistical uncertainty is 30% in the calculated value of the parameters. [b] The dissociation constant of calcium from interface free forms of the enzyme. [c] In the absence of calcium the alkylation time is used to derive the apparent affinity of Ca-free PLA2 for deoxy-LPC (*36*).

the inactivation time (t_E) by alkylation of His-48 by *p*-nitro-phenacylbromide differ by a factor of 5 for the eng-mutants. Also the K_{Ca} values for the E form obtained from the calcium dependent increase in the alkylation time are in the 0.14 mM (eng-IB) to 1.5 mM (eng-IIA) range. These results suggest that the overall effect of the change in the disulfide architecture on the calcium affinity of the E form of the eng-mutants is 10-fold: The M8,20L substitution increases the affinity by a factor of 2.5, whereas the change in the disulfide architecture decreases the affinity for calcium by up to a factor of 10.

In the presence of deoxy-LPC but in the absence of calcium the alkylation time decreases marginally such that the apparent affinity $K_{ND}^*(-Ca)$ for deoxy-LPC is >1 mole fraction (Table 3). This means that in the absence of calcium the affinity of deoxy-LPC for the active site of all the mutants bound to the deoxy-LPC dispersions ($X_I^* = 1$) is insignificant. Virtually the same results were obtained with PN16 and D-LPC. On the other hand, as summarized in Table 2, the X_I^{50*} values for the phosphocholines decrease significantly in the presence of calcium, although the magnitude of the change is not the same for all the mutants.

Binding of Decylsulfate to the i-Face. Binding of mono-disperse decylsulfate (*31, 38*) to eng-mutants was monitored to characterize the possible changes in the amphiphile
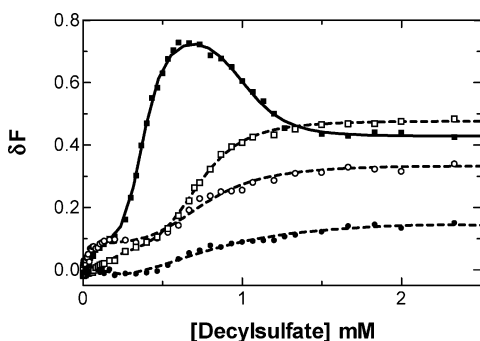
FIGURE 4: Increase in the relative Trp-3 fluorescence emission intensity ($F/F_o - 1 = \delta F$) at 333 nm (excitation at 280 nm) from 2 μM (squares) iso-PLA2 or (circles) eng-X in (filled symbols) 0.5 mM calcium or (unfilled symbols) 1 mM EGTA as a function of monodisperse decylsulfate (CMC 4.5 mM) concentration. The fit parameters (nine for the three-step binding in eq 1) are summarized in Table 4.

interactions along the i-face (*13*). The absorbance and fluorescence spectra of Trp-3 in the eng-mutants in the aqueous phase are noticeably different (results not shown). Also the effect of calcium on the fluorescence emission is modest. However, as shown in Figure 4, a stepwise change in the relative emission intensity of Trp-3 of two of the mutants at 333 nm is observed as a function of added monodisperse decylsulfate (CMC 4.5 mM) in the presence and absence of calcium. In Figure 4, three steps are clearly distinguishable for iso-PLA2 in the presence of calcium, and the third step for most other mutants is discernible in the 2.5 to 4 mM range. Virtually no additional change was observed above the CMC (4.5 mM) for any of the mutants. The titration curves are interpreted as the cooperative binding of decylsulfate to the i-face of PLA2 to sequentially form three premicellar $E_i^{\#}$ complexes (*13, 31*):

$$ E \xrightarrow{n_1, K_1} E_1^{\#} \xrightarrow{n_2, K_2} E_2^{\#} \xrightarrow{n_3, K_3} E_3^{\#} \qquad (2) $$
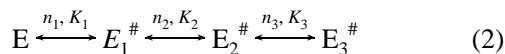
Each binding step is described by a Hill parameter n_i and a dissociation constant K_i ($i = 1, 2, 3$). Assuming that the signal from the complex $E_1^{\#}$ is a_1, from $E_2^{\#}$ is a_2, and from $E_3^{\#}$ is a_3, the total signal can be expressed as

$$ S(E_T, c_f) = E_T \frac{(c_f/K_1)^{n_1}\{a_1 + (c_f/K_2)^{n_2}[a_2 + a_3(c_f/K_3)^{n_3}]\}}{1 + (c_f/K_1)^{n_1}\{1 + (c_f/K_2)^{n_2}[1 + (c_f/K_3)^{n_3}]\}} \qquad (3) $$

where E_T is the total concentration of enzyme and c_f is the concentration of free decylsulfate. When decylsulfate is in large excess over enzyme, the depletion of free amphiphile due to the complex formation can be neglected and c_f in eq 3 can be replaced by the total concentration c. If the three binding steps are well separated, the nine parameters n_1, n_2, n_3, K_1, K_2, K_3, a_1, a_2, and a_3 can be estimated. If only two binding steps contribute, the result is given by eq 3 where all terms $(c_f/K_3)^{n_3}$ for the first step are set to zero. These relations hold when the amphiphile concentration is in large excess over enzyme and therefore the amphiphile depletion is not significant.

The fit parameters for the titration of the mutants up to 3.6 mM added decylsulfate with and without calcium are summarized in Table 4. Amplitudes (the a_i values in Table

4) of the fluorescence changes associated with the formation of each of the $E_i^{\#}$ complexes are significantly different. Uncertainties in values of K_i and n_i are related to the magnitude of the corresponding a_i value. For a change of <0.05 in a_i, the n_i and K_i values are only guesses consistent with the data. Hill coefficient n_1 for the first step is typically about 2 for most mutants. The n_2 values decrease from about 8−10 to 3−5 for some mutants. These differences are significant because in virtually all cases the change in a_2 is significant (>0.3). Since the change from a_2 to a_3 is modest and occurs in the 2 to 3.5 mM concentration range, the n_3 values in the 8 to 15 range should be considered indistinguishable. Note that the M8,20L substitution decreases the a_i values and a modest further increase is seen with the eng-IIA.

The decylsulfate K_i values for the eng-mutants differ marginally. The most significant difference is in the K_2 and K_3 values for iso-PLA2 (A12T,H15D,M20L,E71N mutant of WT) where the effect of calcium on K_2 and K_3 is also significant. In virtually all other cases the effect of mutation as well of the presence of calcium is marginal at best. The decrease from a_2 to a_3 for the formation of $E_3^{\#}$ is also the largest with isoPLA2 in the presence of calcium. This is also the only mutant for which the effect of calcium on the K_2 and K_3 values is significant. Together these results show that the affinity of monodisperse decylsulfate for the i-face of eng-mutants does not change significantly, i.e. the effect of the disulfide architecture on the stability of the premicellar complexes is negligible.

Binding and Displacement of TMA-DPH. As shown in Figure 5A, *p*-trimethylammonium diphenylhexatriene (TMA-DPH) binds with high affinity to PLA2 and the apparent affinity depends modestly on the disulfide architecture. As shown in Figure 5B, a biphasic change is observed on titration of the equimolar mixture of PLA2 and TMA-DPH with decylsulfate. The initial decrease is seen only with the enzyme containing the Trp-3 residue. It suggests a loss of the energy transfer signal as the TMA-DPH bound to the enzyme is displaced by decylsulfate to form the higher premicellar complexes $E_1^{\#}$. On further addition of decylsulfate the signal increases. Our interpretation is that the signal in the rising phase is due to the partitioning of TMA-DPH into the cluster of amphiphiles in the premicellar complex $E_2^{\#}$. After the dilution of PLA2 from the probe in the $E_3^{\#}$ complex with micellar decylsulfate, only the signal from the probe in micelles remains (*13, 31, 38*). A modest signal in the rising phase due to the partitioning in the $E_2^{\#}$ form of W3F mutant is consistent with this interpretation.

Interpretation of both the phases of the TMA-DPH signal is consistent with the model in eq 2. From the TMA-DPH desorption assay the parameters for the formation of $E_1^{\#}$ and $E_2^{\#}$ from the results in Figure 5B are summarized in Table 4. In the presence of the probe the K_1 and K_2 as well as the n_1 and n_2 values are marginally lower than those obtained from the change in the Trp emission. However, note that the relative changes in the RET signal are considerably different for the eng-mutants. Higher RET efficiency in the $E_2^{\#}$ complex of the engineered mutants would be consistent with the suggestion that the TMA-DPH binding site is near the i-face and it is enhanced by the M8,20L change in all the eng-mutants.

Table 4: The Decylsulfate Binding Parameter for the IB eng-Mutants[a]

mutant	Ca[b]	TMA-da[c]	K_1	K_2	K_3	a_1	a_2	a_3	n_1	n_2	n_3
WT	+	−	0.077	0.93	2.4	0.27	0.66	0.59	1.9	9.6	10
	−	−	0.03	0.77	2.8	0.24	0.57	0.50	1.9	8	12
	+	+	0.06	0.64		−0.9	2.2		2.2	2.1	
iso-PLA2	+	−	0.2	0.36	1.0	0.2	0.77	0.43	1.0	5.7	8
	−	−	0.19	0.72	>3	0.07	0.48	0.34	3.1	5.1	10
M8,20L	+	−		0.64	3.3		0.20	0.12		12	16
	−	−	0.03	0.8	1.67	0.086	0.26	0.32	2.1	10.8	15
	+	+	0.04	0.49		−0.72	0.27		1.3	5.4	
eng-IIA	+	−	0.18	0.69	>3	0.21	0.44		1.7	8.3	
	−	−	0.23	0.75	>3	0.13	0.45	0.4	2.3	5.4	
	+	+	0.08	0.59		−0.61	1.3		2.5	4.7	
eng-IIC[#]	+	−	0.09	0.53	2.5	0.04	0.12	0.23	2.8	4.6	8
	+	−		0.83	2.8		0.16	0.11		2.8	15
	−	−	0.02	0.76	3.7	0.09	0.33	0.27	1.3	4	10
	+	+	0.04	0.53		−0.83	0.36		1.5	4.7	

[a] The fitting of decylsulfate cooperative binding values is described in eqs 2 and 3, where $i = 1$, 2, or 3 and n_i is the Hill parameter, K_i is the dissociation constant, and a_i represents the signal from enzyme form E_i. K_i values are in mM. Statistical uncertainty is 30% in the calculated value of the parameters. [b] These measurements were carried out (+) in 0.5 mM Ca or (−) in 1 mM EGTA. [c] (+) Results from the desorption assay monitored as resonance energy transfer signal to TMA-DPH (see Figure 5).
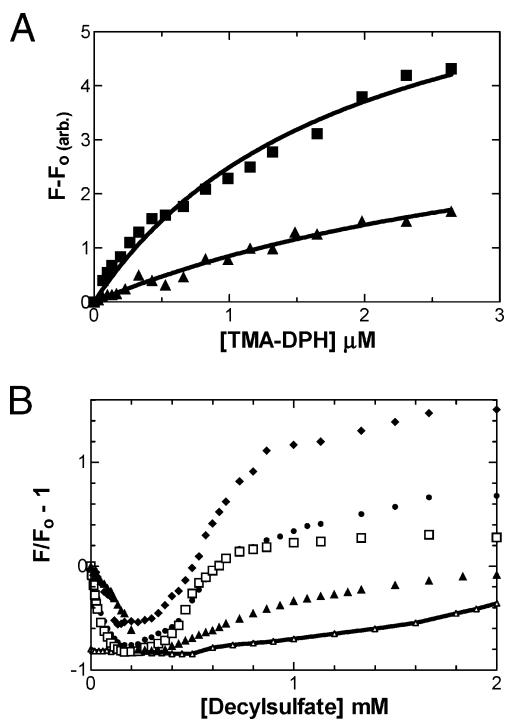

FIGURE 5: (A) Net change in the RET emission intensity of TMA-DPH in the presence of 1 μM (square) WT PLA2 with fit for K_d 1.9 ± 0.3 μM or (triangles) eng-X with fit for K_d 4.1 ± 0.6 μM. (B) Change in the energy transfer signal from TMA-DPH (ex 280, em 450 nm) from a mixture of 1 μM TMA-DPH and 1 μM PLA2 (triangle) WT, (square) eng-IB; (diamond) eng-IIA; (circle) eng-X; (connecting line) W3F mutant of WT titrated with decylsulfate.

Table 5: X-ray Data Collection and Refinement of eng-X PLA2 Structures

	eng-X	
	no ligand	with MJ33
Crystal Data		
space group	$P2_1$	$P2_1$
cell params		
a (Å)	35.0	38.5
b (Å)	88.4	85.9
c (Å)	38.6	38.6
β (deg)	105.7	94.8
subunits/asymmetric unit	2	2
X-ray Data		
total reflections	65225	128590
unique reflections	10213	14777
resolution limit (Å)	2.20	2.00
completeness (%)	95.2 (90.8)[a]	87.1 (83.3)[b]
R_{merge} (%)[c]	11.3 (32.3)[a]	6.1 (31.6)[b]
Refinement		
resolution range (Å)	19.8−2.25	28.6−2.00
$R_{working}$[d]	0.191 (0.232)[e]	0.196 (0.248)[b]
R_{free}[d]	0.265 (0.296)[e]	0.245 (0.318)[b]
RMSD observed		
bond length (Å)	0.006	0.005
angle (deg)	1.2	1.8
total water molecules	216	206
Ramachandran plot regions		
most favored (%)	88.5	90.6
additionally allowed (%)	11.5	9.4

[a] The value in parentheses is for X-ray data from 2.28 to 2.20 Å. [b] The value in parentheses is for X-ray data from 2.07 to 2.00 Å. [c] $R_{merge} = \Sigma|I_o - I_a|/\Sigma(I_a)$, where I_o is the observed intensity and I_a is the average intensity, the sums being taken over all symmetry related reflections. [d] R-factor $= \Sigma|F_o - F_c|/\Sigma(F_o)$, where F_o is the observed amplitude and F_c is the calculated amplitude. R_{free} is the equivalent of $R_{working}$, except it is calculated for a randomly chosen set of reflections that were omitted (10%) from the refinement process (20). [e] The value in parentheses is for X-ray data from 2.39 to 2.25 Å.

Structures of eng-X PLA2. Crystal structures of eng-X PLA2 with and without MJ33 in the active site provide support for the functional differences described above. Table 5 summarizes the data collection and structural refinement statistics of the 2.25 Å structure (which had no active site ligand bound) and the 2.0 Å structure (which had the active site directed ligand MJ33 in the active site). As expected, the protein folds of both the eng-X structures are quite similar to previously reported PLA2 structures (8, 39, 40). These structures also support the expected disulfide bonding pattern of the hX PLA2. The design of the disulfide between residues 50 and 131 is cleanly modeled in this structure. As expected,

the active site of the eng-X structure is remarkably similar to the previously solved group-IB (39) group-IIA (40), and group-X (8) enzymes. This is expected because residues of the active site are highly conserved.

Subtle structural differences are noteworthy because they provide information about the interfacially activated state of PLA2. The MJ33-bound form of eng-X crystallized in an anion-assisted dimer form. The asymmetric unit contained
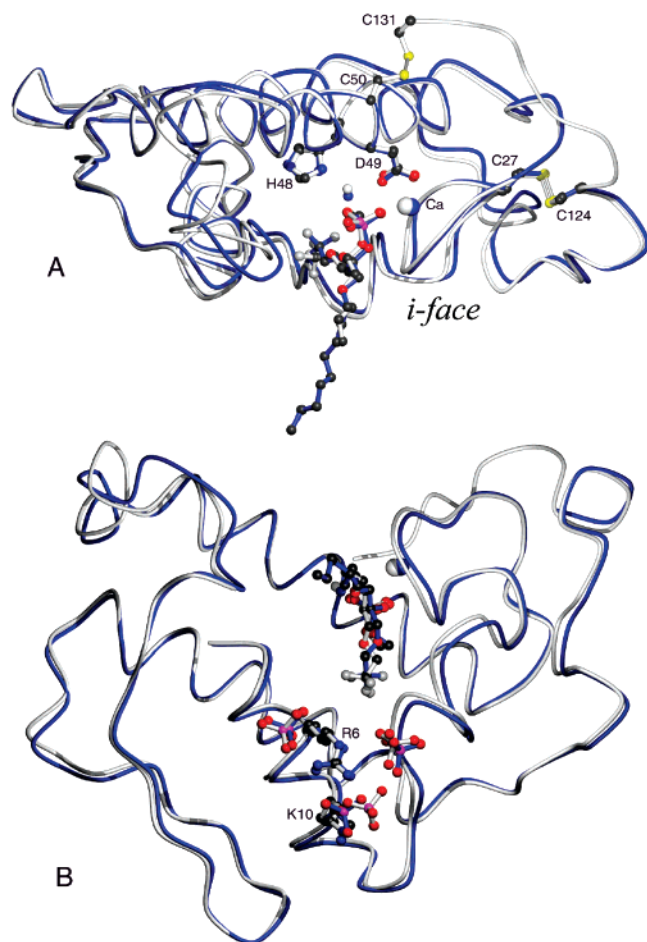
FIGURE 6: Overlay of porcine eng-X and WT-IB PLA2 in the anion-assisted dimer form and complexed with MJ33. (A) The i-face of PLA2 is pointing down as indicated by the alkyl tail of MJ33. The anion-assisted dimer structure of WT-IB is shown in blue (PDB code 1fxf), and eng-X PLA2 is shown in gray. The C-terminal extension of eng-X is displayed between C124 and C131, with these two disulfide bonds labeled for eng-X. Also shown in the active site are the Ca, H48, D49, and the assisting water, $w7$, which bridges MJ33 and H48 of each structure. (B) Rotated 90° from panel A such that the i-face of PLA2 is facing outward. MJ33 and Ca are displayed in the active site of this view. Three bound phosphate anions from each structure are shown relative to R6 and K10 with the WT-IB enzyme's Ca, MJ33, and 3 phosphates shown in blue and the eng-X protein's Ca, MJ33, and 3 phosphates shown in gray.

2 copies of the protein subunit, bound with Ca^{2+} and MJ33 in the active site. The crystal contacts of this crystal form placed these two neighboring subunits with interactions similar but not identical to the previously published anion-assisted dimer of wild-type PLA2 (*7*). Just as in the wild-type anion-assisted dimer structure (*7*), the i-face interaction in the eng-X/MJ33 structure is involved in the packing of each subunit facing each other. Located within a plane between these subunits were 3 bound phosphate anions. As shown in Figure 6, the arrangement of protein subunits, MJ33, and phosphate anion is strikingly similar to the anion-assisted dimer form of the wild-type group-IB PLA2 bound with MJ33 and 5-coplanar phosphate anions (*7*). In comparison to the wild-type IB anion-assisted dimer, the arrangement of one subunit to the other is shifted due to the addition at the C-terminus of the eng-X enzyme. Despite this perturbation, the eng-X has adopted the anion-assisted dimer form; however, two of the phosphate anions in the
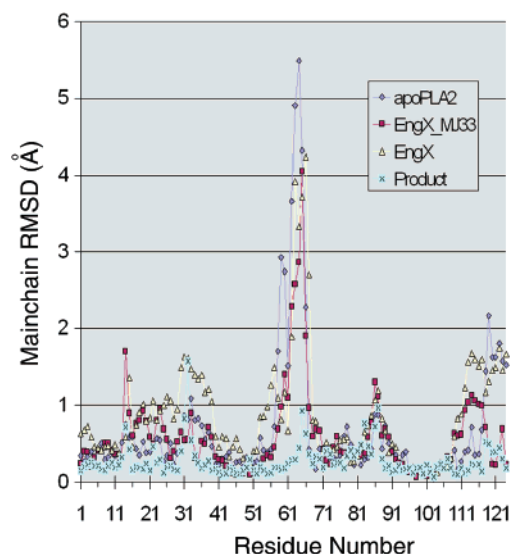

FIGURE 7: Comparison of main chain C_α atoms from an alignment of the anion-assisted dimer structure of wild-type pIB with MJ33 bound (*7*), the anion-assisted dimer structure with product-acetate (cross) (*46*), the anion-assisted dimer form of eng-X with MJ33 bound (square), ligand free eng-X (triangle), and a ligand free form of porcine wild-type group-IB (diamond, unpublished). The RMSD differences are displayed for the C_α atom of the aligned structures relative to the wild-type anion assisted structure (PDB code 1fxf).

WT PLA2 structure bound to K120 are not seen in the eng-X structure.

The active site of the eng-X MJ33 structure has a 7-coordinate Ca and a water molecule, $w7$, bridging the MJ33 ligand and His-48, just as in the anion-assisted dimer structure of the pig IB PLA2 (*7*). An RMSD difference plot of the eng-X/MJ33-bound structure with the IB anion-assisted dimer and the ligand free eng-X PLA2 structure is shown in Figure 7. The most notable deviation in the Cα backbone is seen in the 69-loop, where the eng-X/MJ33 structure has a loop placement that is intermediate between a wild-type IB anion-assisted dimer and the ligand free monomer structure of eng-X. The other notable difference is seen at the C-terminus. Although a comparison could not be made for the extension added to the eng-X enzyme, the residues from 116 to 124 show a notable difference between the anion-assisted forms and the monomer form of the enzyme.

The ligand free structure of eng-X PLA2 is also remarkably similar to the ligand free structure of group-IB PLA2 in a monomer protein crystal form (*39*). This crystal form, without an active site ligand bound, did not crystallize as an anion-assisted dimer. An alignment of the ligand free eng-X has been performed against the human group-X PLA2 structure (*8*) and is shown in the top panel of Figure 8. The aligned structures show significant differences possibly related to the structural role played by a modified disulfide bonding pattern. The crystal form of the ligand free eng-X structure has two subunits per asymmetric unit and therefore offers two independent views of the structure. In one subunit the calcium ligand Asp-49 can be seen rotated away from the calcium position (Figure 8). In each subunit the B-factor of the calcium is high (58 and 50 $Å^2$). The refined data suggests a partially bound Ca^{2+} structure, which will be discussed below in connection with observed kinetic results for the eng-X enzyme.
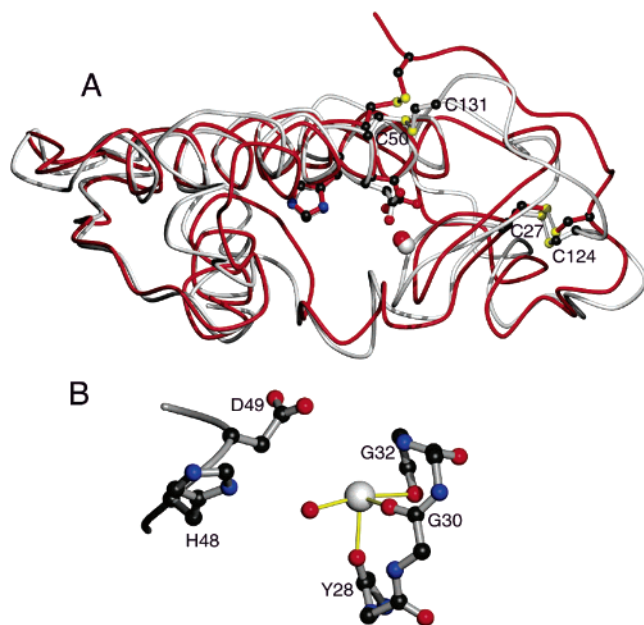
FIGURE 8: Comparison of the ligand free eng-X to the natural hX PLA2 enzyme. (A) Overlay of ligand free forms of eng-X shown in white with human group-X PLA2 shown in red (PDB 1le6). The C-terminal portion of these structures is highlighted by the eng-X PLA2 disulfides C124−C27 and C131−C50, which correspond to the human group-X PLA2 disulfides C115−C25 and C122−C48, respectively. (B) The Ca coordination in MJ33-free eng-X shows a four-coordinate Ca site. The usual Ca-ligand D49 is not coordinated to Ca in subunit-A of this structure with its Ca *B*-factor of 58 Å^2. Although subunit-B of eng-X PLA2 has D49 coordinated to the Ca, the *B*-factor of 50 Å^2 is indicative of a low occupancy binding, just as in subunit-A of this structure.

DISCUSSION

Our analysis of the eng-mutants with pig IB PLA2 sequence shows that changing the disulfide architecture has a modest effect on the turnover and the interfacial binding parameters. The most significant effect, about 10-fold, is on the affinity of the enzyme in solution for calcium. A significant effect on the active site-directed binding of phosphocholines is also noted, and this may be related to the relative affinity of glycerophosphocholine headgroup to the i-face (for a surface diluent) versus the active site (for an inhibitor). On the other hand, as expected (*26*), the effect of the change in the disulfide architecture on the binding to anionic interface or the allosteric activation of k_{cat}* is not significant. The modest effect on the interfacial turnover rate can be attributed to the affinity of the bound enzyme for the substrate in the interface, i.e. the interfacial K_M*. Together, the disulfide architecture could at best only moderately influence the functional state of the enzyme at the anionic interface, whereas the solution form of the disulfide mutants may be significantly different. It is also likely that the surface architecture of PLA2 controlled by the disulfide architecture could play a more prominent physiological role in receptor recognition. Although little is known about the receptor specificity of mammalian sPLA2 (*3*), such interactions could contribute toward their apparent specificity for the target tissue.

Virtually all the functional changes observed in the disulfide engineered mutants can be explained by a slight change in the active site architecture. A comparison of the eng-mutants with the corresponding human homologue

suggests a measurable effect of the disulfide architecture (Figure 1) on the interfacial turnover rate (Table 1). Less than 30-fold difference in the observed rate corresponds to roughly 2 kcal in the elemental event. Most, if not all, of this effect can be attributed to the modest change in the calcium affinity for the E form (Table 3 and Figure 8). The apparent affinity of the ligand is calcium concentration dependent (*36*, *41*). For example the apparent dissociation constant for a ligand at a subsaturating concentration of calcium is related to K_{Ca}* for the dissociation of ECa, and K_L* for the dissociation of L from E*Ca·L as

$$K_L^*(Ca) = K_L^* (1 + K_{Ca}^*/[Ca]) \qquad (4)$$

Similarly, the apparent dissociation constant for calcium at the mole fraction X_L* of a ligand is

$$K_{Ca}^*(L) = K_{Ca}^*/(1 + X_L^*/K_L^*) \qquad (5)$$

Here, the apparent kinetic K_M*(Ca) is related to K_{Ca}* and intrinsic K_M* for the interfacial turnover cycle at saturating calcium (*2*).

If calcium is an obligatory cofactor for the binding of the active site directed ligands to PLA2, a perturbation in the calcium binding would also influence the transition state. This is useful for understanding the origin of the functional differences between the eng-mutants. For example, for a ligand with strong affinity the apparent saturating concentration of calcium will be lower. If the affinity of the mutant for calcium decreases, K_L*(Ca) would increase. Also for the tight binding ligands with low K_L* the effect of mutation on K_{Ca}* would be insignificant. On the other hand, for the weaker ligands with larger K_L* the effect of an increase in K_{Ca}* would be more noticeable. Since a significant effect of mutation is seen only for the weaker active site directed ligands (Table 2), we believe that the key difference in these eng-mutants is in the effective calcium dependent substrate affinity. These assertions based on the theoretical predictions from the interfacial catalysis model for PLA2 (*1*, *2*) are qualitatively consistent with the results in Tables 1 and 2. However, quantitative resolution of the underlying elementary equilibria would require a perfect diluent for each of the mutants, which we do not currently have. Also note that these relations hold for all calcium requiring secreted PLA2 that share the Ca-His-Asp motif in the active site. Of course, the relative magnitudes of the primary and apparent dissociation constants will be different.

It is established that the group-IB and -IIA PLA2 do not require calcium for the binding to the interface (*1*, *2*). On the basis of the results for the formation of $E_i^\#$ complexes, it appears that this may also be the case for other secreted PLA2s. Results with eng-mutants show that the disulfide architecture has little effect on the amphiphile binding to the i-face. Therefore the interface preference associated with the i-face must be a property of the side chains on the i-face. Spectroscopic results show that the affinity of zwitterionic PC$_6$-ether to the i-face of eng-mutants is weak and comparable to that for the WT. On the other hand, the affinity of PC$_6$-ether for the i-face of human PLA2s is noticeably higher (Figure 2). Formation of the premicellar aggregates under these conditions also accounts for the significant turnover with monodisperse DC$_7$PC (Table 1).

The group-IB PLA2 has a preference for the anionic interface. This is supported by the result that monodisperse decylsulfate binds to the i-face of all the eng-mutants (Table 4) to form three discrete premicellar complexes. Although calcium has a modest effect on the fluorescence emission from Trp-3 in these complexes, the effect of calcium on the Hill numbers n_i and K_i is marginal, if at all. The effect of the M8,20L substitution and disulfide architecture on the Trp environment and the active site events suggest a common structural origin. The A12T,H15D,M20L substitutions in iso-PLA2 also influence the Trp-3 emission. We attribute such structural effects on the Trp-3 emission environment to the changes in the N-terminal-helix (residues 1−12). Changes in the helix are likely to be communicated to the conserved H-bonding network that links the N-terminal helix to the active site (*42*). On the basis of the following circumstantial evidence we suggest that changes in the i-face and the resulting changes in the H-bonding network could be coupled to the active site events.

(a) Side chains of Ala-1 and Gln-4 are part of the H-bonding network via the highly conserved structural water molecule w1.

(b) Phe-5 makes contact with a CH_2 near the ester group of the *sn*-2-acyl chain (*43*, *44*), and Ile-2 also makes contact with the *sn*-2 chain (*45*).

(c) Asn-71 and Pro-68 coupled to w1 could influence the interactions of Y69 and the orientation of the 69-loop (Figure 7) and the H-bonding of the Y69 −OH group to the *sn*-3-phosphate of the substrate. Such interactions could not be seen in comparing the eng-X/MJ33 complex with eng-X-ligand free form, and in comparing the anion-assisted dimer of MJ33+WT PLA2 with the ligand free form. This is not surprising because MJ33 does not contain the *sn*-3-phosphate.

(d) The other end of the H-bonding network controls the side chain carbonyl of Asp-99 as an integral part of the His-48-Asp-99 catalytic dyad. Its role in the formation of the premicellar complexes is indicated in the behavior of D99A mutant (*38*).

Structural Effects. Considerations outlined above are useful for structural rationalization of the functional and spectroscopic changes. A useful lead is provided by a comparison of the crystal structure of eng-X with the corresponding structure of pig IB PLA2. Most of the structural differences in the root-mean-square distances are well within 2 Å (Figure 7), although the difference in the 69-loop and the calcium coordination environment of the E form is significant. The anion-assisted dimer structure with occupied active site has been previously reported for the wild-type pig IB PLA2 under two different conditions (*7*, *46*), and in the present work with eng-X. However, the C-terminal extension in the eng-X structure makes the arrangement of subunits somewhat different from that of the wild-type IB dimer. In all cases, phosphate anions and an active ligand bring two subunits together with their i-faces in contact with each other. The position of the 69-loop is affected by this arrangement. In addition, the structural differences highlighted in the calcium-binding loop are likely to have a more significant connection to functional results. The structural results also support a weakened affinity of eng-X for calcium with a displaced D49 in one subunit, and a high B-factor for the calcium. The functional results suggest that this could influence the binding of the phosphocholine amphiphiles.

Overall, despite significant perturbation of the solution form of eng-X, the similarity of the anion-assisted dimer of eng-X/MJ33 and the wild-type IB/MJ33 structures at the C-terminus highlights the key factors that may lead to the interfacially activated form of PLA2. The eng-X structure also shows significant differences compared to the structure of human group-X (Figure 8). The presence or absence of the anion-assisted dimer crystal form has a greater structural effect on PLA2 structure than changing the disulfide bonding pattern from IB to X. As shown in Figure 1, the five core disulfide bonds shown in green are expected to have a more significant impact on the active site and catalytic properties. Among the engineered and natural human paralogues, the three variant disulfide bonds are peripheral to the active site, and therefore are not expected to play as significant a factor in kinetic function. By extension to the kinetic results of the other eng-mutants, this structural argument will likely hold true for the other disulfide bonding modifications reported elsewhere (*47*).

REFERENCES

1. Berg, O. G., and Jain, M. K. (2002) *Interfacial Enzyme Kinetics*, Wiley, London.
2. Berg, O. G., Gelb, M. H., Tsai, M. D., and Jain, M. K. (2001) Interfacial enzymology: the secreted phospholipase A2-paradigm, *Chem. Rev. 101*, 2613−54.
3. Valentin, E., and Lambeau, G. (2000) Increasing molecular diversity of secreted phospholipases A(2) and their receptors and binding proteins, *Biochim. Biophys. Acta 1488*, 59−70.
4. Six, D. A., and Dennis, E. A. (2000) The expanding superfamily of phospholipase A(2) enzymes: classification and characterization, *Biochim. Biophys. Acta 1488*, 1−19.
5. Singer, A. G., Ghomashchi, F., Le Calvez, C., Bollinger, J., Bezzine, S., Rouault, M., Sadilek, M., Nguyen, E., Lazdunski, M., Lambeau, G., and Gelb, M. H. (2002) Interfacial kinetic and binding properties of the complete set of human and mouse groups I, II, V, X, and XII secreted phospholipases A2, *J. Biol. Chem. 277*, 48535−49.
6. Janssen, M. J., Verheij, H. M., Slotboom, A. J., and Egmond, M. R. (1999) Engineering the disulphide bond patterns of secretory phospholipases A2 into porcine pancreatic isozyme. The effects on folding, stability and enzymatic properties, *Eur. J. Biochem. 261*, 197−207.
7. Pan, Y. H., Epstein, T. M., Jain, M. K., and Bahnson, B. J. (2001) Five coplanar anion binding sites on one face of phospholipase A2: relationship to interface binding, *Biochemistry 40*, 609−17.
8. Pan, Y. H., Yu, B. Z., Singer, A. G., Ghomashchi, F., Lambeau, G., Gelb, M. H., Jain, M. K., and Bahnson, B. J. (2002) Crystal structure of human group X secreted phospholipase A2. Electrostatically neutral interfacial surface targets zwitterionic membranes, *J. Biol. Chem. 277*, 29086−93.
9. Nieuwenhuizn, W., Steenbergh, P., and de Haas, G. (1973) The isolation and properties of two prephospholipase A2 from porcine pancreas, *Eur. J. Biochem. 40*, 1−7.
10. Jain, M. K., Rogers, J., Jahagirdar, D. V., Marecek, J. F., and Ramirez, F. (1986) Kinetics of interfacial catalysis by phospholipase A2 in intravesicle scooting mode, and heterofusion of anionic and zwitterionic vesicles, *Biochim. Biophys. Acta 860*, 435−47.
11. Berg, O. G., Yu, B. Z., Rogers, J., and Jain, M. K. (1991) Interfacial catalysis by phospholipase A2: determination of the interfacial kinetic rate constants, *Biochemistry 30*, 7283−97.
12. Berg, O. G., Rogers, J., Yu, B. Z., Yao, J., Romsted, L. S., and Jain, M. K. (1997) Thermodynamic and kinetic basis of interfacial activation: resolution of binding and allosteric effects on pancreatic phospholipase A2 at zwitterionic interfaces, *Biochemistry 36*, 14512−30.
13. Berg, O. G., Yu, B. Z., Chang, C., Koehler, K. A., and Jain, M. K. (2004) Cooperative binding of monodisperse anionic amphiphiles to the i-face: Phospholipase A2-paradigm for interfacial binding, *Biochemistry 43*, 7999−8013.

14. Jancarik, J., and Kim, S. H. (1991) Sparse matrix sampling: a screening method for crystallization of proteins, *J. Appl. Crystallogr. 24*, 409−11.

15. Otwinowski, Z., and Minor, W. (1997) Processing of x-ray diffraction data collected in oscillation mode, *Methods Enzymol. 276*, 307−26.

16. Navaza, J. (2001) Implementation of molecular replacement in AMoRe, *Acta Crystallogr., Sect. D: Biol. Crystallogr. 57*, 1367−72.

17. Brunger, A. T., Adams, P. D., Clore, G. M., Delano, W. L., Gros, P., Grosse-Kunstleve, R. W., Jiang, J.-S., Kuszewski, J., Nilges, N., Pannu, N. S., Read, R. J., Rice, L. M., Simonson, T., and Warren, G. L. (1998) Crystallography and NMR systems (CNS): A new software system for macromolecular structure determination, *Acta Crystallogr. D54*, 905−21.

18. Sack, J. S., and Quiocho, F. A. (1997) CHAIN: A crystallographic modeling program, *Methods Enzymol. 277*, 158−73.

19. Jones, T. A., Zou, J. Y., Cowan, S. W., and Kjeldgaard, M. (1991) Improved methods for building protein models in electron density maps and the location of errors in these models, *Acta Crystallogr., Sect. A 47*, 110−9.

20. Brunger, A. T. (1992) The free *R* value: A novel statistical quantity for assessing the accuracy of crystal structures, *Nature 355*, 472−4.

21. Cajal, Y., Rogers, J., Berg, O. G., and Jain, M. K. (1996) Intermembrane molecular contacts by polymyxin B mediate exchange of phospholipids, *Biochemistry 35*, 299−308.

22. Jain, M. K., Rogers, J., Berg, O., and Gelb, M. H. (1991) Interfacial catalysis by phospholipase A2: activation by substrate replenishment, *Biochemistry 30*, 7340−8.

23. Cajal, Y., Berg, O. G., and Jain, M. K. (1995) Direct vesicle-vesicle exchange of phospholipids mediated by polymyxin B, *Biochem. Biophys. Res. Commun. 210*, 746−52.

24. Cajal, Y., Rogers, J., Berg, O. G., and Jain, M. K. (1996) Intermembrane molecular contacts by polymyxin B mediate exchange of phospholipids, *Biochemistry 35*, 299−308.

25. Rogers, J., Yu, B. Z., Tsai, M. D., Berg, O. G., and Jain, M. K. (1998) Cationic residues 53 and 56 control the anion-induced interfacial k*cat activation of pancreatic phospholipase A2, *Biochemistry 37*, 9549−56.

26. Yu, B. Z., Poi, M. J., Ramagopal, U. A., Jain, R., Ramakumar, S., Berg, O. G., Tsai, M. D., Sekar, K., and Jain, M. K. (2000) Structural Basis of the Anionic Interface Preference and Activation of Pancreatic Phospholipase A(2), *Biochemistry 39*, 12312−23.

27. Beers, S. A., Buckland, A. G., Koduri, R. S., Cho, W., Gelb, M. H., and Wilton, D. C. (2002) The antibacterial properties of secreted phospholipases A2: a major physiological role for the group IIA enzyme that depends on the very high pI of the enzyme to allow penetration of the bacterial cell wall, *J. Biol. Chem. 277*, 1788−93.

28. Beers, S. A., Buckland, A. G., Giles, N., Gelb, M., and Wilton, D. C. (2003) Effect of tryptophan insertion on th properties of human group IIA phospholipase A_2: Mutagenesis produced an enzyme with characteristics similar to those of the group V phospholipase A_2, *Biochemistry 42*, 7326−38.

29. Jain, M. K., Tao, W. J., Rogers, J., Arenson, C., Eibl, H., and Yu, B. Z. (1991) Active-site-directed specific competitive inhibitors of phospholipase A2: novel transition-state analogues, *Biochemistry 30*, 10256−68.

30. Yu, B. Z., Berg, O. G., and Jain, M. K. (1999) Hydrolysis of monodisperse phosphatidylcholines by phospholipase A2 occurs on vessel walls and air bubbles, *Biochemistry 38*, 10449−56.

31. Berg, O. G., Yu, B. Z., Apitz-Castro, R. J., and Jain, M. K. (2004) Phosphatidylinositol-specific phospholipase C forms different complexes with monodisperse and micellar phosphatidylcholine, *Biochemistry 43*, 2080−90.

32. Jain, M. K., Rogers, J., Hendrickson, H. S., and Berg, O. G. (1993) The chemical step is not rate-limiting during the hydrolysis by phospholipase A2 of mixed micelles of phospholipid and detergent, *Biochemistry 32*, 8360−7.

33. Jain, M. K., Ranadive, G., Yu, B. Z., and Verheij, H. M. (1991) Interfacial catalysis by phospholipase A2: monomeric enzyme is fully catalytically active at the bilayer interface, *Biochemistry 30*, 7330−40.

34. Yu, B. Z., Rogers, J., Nicol, G. R., Theopold, K. H., Seshadri, K., Vishweshwara, S., and Jain, M. K. (1998) Catalytic significance of the specificity of divalent cations as KS* and kcat* cofactors for secreted phospholipase A2, *Biochemistry 37*, 12576−87.

35. Jain, M. K., Yu, B. Z., Rogers, J., Smith, E., Boger, E. T. A., Ostrander, R. L., and Rheingold, A. L. (1995) Specific competitive inhibito of secreted phospholipase A_2 from berries of *Schnscinius terebinthifolius*, *Phytochemistry 39*, 537−47.

36. Yu, B. Z., Berg, O. G., and Jain, M. K. (1993) The divalent cation is obligatory for the binding of ligands to the catalytic site of secreted phospholipase A2, *Biochemistry 32*, 6485−92.

37. Yu, B. Z., Ghomashchi, F., Cajal, Y., Annand, R. R., Berg, O. G., Gelb, M. H., and Jain, M. K. (1997) Use of an imperfect neutral diluent and outer vesicle layer scooting mode hydrolysis to analyze the interfacial kinetics, inhibition, and substrate preferences of bee venom phospholipase A2, *Biochemistry 36*, 3870−81.

38. Yu, B. Z., Apitz-Castro, R., Tsai, M. D., and Jain, M. K. (2003) Interaction of monodisperse anionic amphiphiles with the i-face of secreted phospholipase A2, *Biochemistry 42*, 6293−301.

39. Steiner, R. A., Rozeboom, H. J., de Vries, A., Kalk, K. H., Murshudov, G. N., Wilson, K. S., and Dijkstra, B. W. (2001) X-ray structure of bovine pancreatic phospholipase A2 at atomic resolution, *Acta Crystallogr., Sect. D: Biol. Crystallogr. 57*, 516−26.

40. Scott, D. L., White, S. P., Browning, J. L., Rosa, J. J., Gelb, M. H., and Sigler, P. B. (1991) Structures of free and inhibited human secretory phospholipase A2 from inflammatory exudate, *Science 254*, 1007−10.

41. Yu, B. Z., Rogers, J., Ranadive, G., Baker, S., Wilton, D. C., Apitz-Castro, R., and Jain, M. K. (1997) Gossypol modification of Ala-1 of secreted phospholipase A2: a probe for the kinetic effects of sulfate glycoconjugates, *Biochemistry 36*, 12400−11.

42. Dijkstra, B. W., Kalk, K. H., Hol, W. G., and Drenth, J. (1981) Structure of bovine pancreatic phospholipase A2 at 1.7 Å resolution, *J. Mol. Biol. 147*, 97−123.

43. Thunnissen, M. M., Ab, E., Kalk, K. H., Drenth, J., Dijkstra, B. W., Kuipers, O. P., Dijkman, R., de Haas, G. H., and Verheij, H. M. (1990) X-ray structure of phospholipase A2 complexed with a substrate-derived inhibitor, *Nature 347*, 689−91.

44. Scott, D. L., White, S. P., Otwinowski, Z., Yuan, W., Gelb, M. H., and Sigler, P. B. (1990) Interfacial catalysis: the mechanism of phospholipase A2, *Science 250*, 1541−6.

45. Liu, X., Zhu, H., Huang, B., Rogers, J., Yu, B. Z., Kumar, A., Jain, M. K., Sundaralingam, M., and Tsai, M. D. (1995) Phospholipase A2 engineering. Probing the structural and functional roles of N-terminal residues with site-directed mutagenesis, X-ray, and NMR, *Biochemistry 34*, 7322−34.

46. Pan, Y. H., Yu, B. Z., Berg, O. G., Jain, M. K., and Bahnson, B. J. (2002) Crystal structure of phospholipase A2 complex with the hydrolysis products of platelet activating factor: equilibrium binding of fatty acid and lysophospholipid-ether at the active site may be mutually exclusive, *Biochemistry 41*, 14790−800.

47. Zhu, H., Dupureur, C. M., Zhang, X., and Tsai, M. D. (1995) Phospholipase A2 engineering. The roles of disulfide bonds in structure, conformational stability, and catalytic function, *Biochemistry 34*, 15307−14.